Multi-valued responses and dynamic stability of a nonlinear vibro-impact system with a unilateral non-zero offset barrier*

Wei Xu(徐伟)[1], Dong-Mei Huang(黄冬梅)[1,2,†], and Wen-Xian Xie(谢文贤)[1]

[1] Department of Applied Mathematics, Northwestern Polytechnical University, Xi'an 710072, China
[2] Department of Civil and Environmental Engineering, Rice University, Houston 77005, USA

(Received 5 August 2015; revised manuscript received 29 September 2015; published online 20 January 2016)

In this paper, multi-valued responses and dynamic properties of a nonlinear vibro-impact system with a unilateral nonzero offset barrier are studied. Based on the Krylov–Bogoliubov averaging method and Zhuravlev non-smooth transformation, the frequency response, stability conditions, and the equation of backbone curve are derived. Results show that in some conditions impact system may have two or four steady-state solutions, which are interesting and not mentioned for a vibro-impact system with the existence of frequency island phenomena. Then, the classification of the steady-state solutions is discussed, and it is shown that the nontrivial steady-state solutions may lose stability by saddle node bifurcation and Hopf bifurcation. Furthermore, a criterion for avoiding the jump phenomenon is derived and verified. Lastly, it is found that the distance between the system's static equilibrium position and the barrier can lead to jump phenomenon under hardening type of nonlinearity stiffness.

Keywords: vibro-impact system, multi-valued response, frequency island, stability

PACS: 05.45.–a, 02.60.Cb **DOI:** 10.1088/1674-1056/25/3/030502

1. Introduction

Vibrating systems or devices with clearance or gaps between moving parts are frequently encountered in the aeronautical, civil, and mechanical engineering fields, particularly in mechanisms and machines,[1,2] such as ships colliding with fenders,[3] rattling of gear boxes,[4] structural interaction in piping systems,[5] and nonlinear soil-structure interaction.[6] This type of systems or devices with repeated impact is called vibro-impact systems or impacting oscillators. Due to the existence of the impact, a vibro-impact system presents strong nonlinearity and discontinuity, accompanied with rich and complicated dynamic behaviors. Therefore, the analyses of the impact motion are important in the proper design of the corresponding machines and devices.[7] Notable contributions were made by many researchers,[8–25] and some interesting phenomena, such as grazing bifurcation,[9] codimension two bifurcation,[11] and torus bifurcation,[14] chatter and sticking motions were observed in the vibro-impact systems.

However, vibro-impact systems, as one kind of non-smooth systems, always have troubles due to their inherent difficulty of analytical study. The main difficulty depends on the additional finite relations between impacts and rebound velocities. On one hand, the impact instants could not predict in advance, but are governed by the equations of motion. Thus, it is reasonable that the impact instants are described by constraints which depend on the state of systems. On the other hand, the impact instants govern the corresponding velocity jumps, i.e., the differential equations of motion on the impact instants are complemented by impact conditions. The previous literatures, which were related to the frequency response of vibro-impact systems, mainly concentrated on traditional frequency responses with single-valued response[16,18] or three-valued response (with jump). However, for more complicated multi-valued responses,[24] such as two-valued and four-valued responses, especially the frequency island phenomenon in the vibro-impact systems, which are not mentioned. For this purpose, we consider the same oscillators as that in Ref. [21], and estimate the multi-valued responses and dynamic properties of the system.

This paper is organized as follows. In Section 2, by using the non-smooth transformation the vibro-impact system is transformed a non-impact system. In Section 3, the Krylov-Bogoliubov averaging method is used to obtain the frequency response equation and the backbone curve equation. By using the linearization method, the stability conditions are derived. In Section 4, the directly numerical simulation is carried out to verify the analytical results obtained in Section 3, the effects of system parameters on the dynamic behaviors are revealed. The classification of the steady-state solutions is discussed. Finally, conclusions are presented in Section 5.

2. Theoretical model and non-smooth transformation

A general nonlinear vibro-impact oscillator with a unilateral nonzero offset barrier is considered, and the schematic model of this oscillator is shown in Fig. 1, where x is the dis-

*Project supported by the National Natural Science Foundation of China (Grant Nos. 11472212, 11532011, 11302171, and 11302172).
†Corresponding author. E-mail: dongmeihuang1@hotmail.com
© 2016 Chinese Physical Society and IOP Publishing Ltd

placement of the mass, $F(t)$ is the external excitation, and h is the distance between the oscillator's static equilibrium position and the rigid barrier. In the following discussion, the non-dimensional equations of the motion are introduced,[21] which are presented as follows:

$$\ddot{x}+\omega_0^2 x+(c_2x^2-c_1)\dot{x}+c_3x^3=F(t), \quad x>-h, \tag{1a}$$

$$\dot{x}_+=-r\dot{x}_-, \quad x=-h, \tag{1b}$$

where dots denote derivatives with respect to time$t$; the parameters ω_0, c_1, and c_2 are assumed to be positive; c_3 is the nonlinear stiffness coefficient; external excitation $F(t)$ is assumed to be $F(t)=f\cos(\Omega t)$; r is the restitution coefficient which depicts impact losses and satisfies $0<r\leq 1$; $\dot{x}_-$ and $\dot{x}_+$ are the velocities of the system before and after the instant of impacts, respectively.

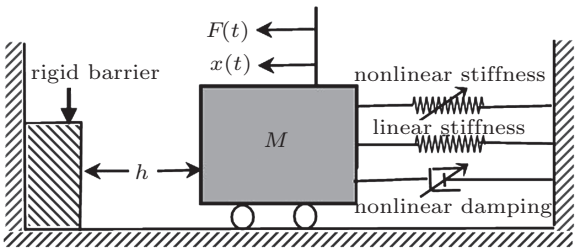


Fig. 1. (color online) Schematic model of the vibro-impact oscillator with a unilateral rigid barrier.

By using the non-smooth transformation[25]

$$x=|y|-h, \quad \dot{x}=\dot{y}\mathrm{sgn}y, \tag{2}$$

where y and $\dot{y}$ are the displacement and velocity of the converted oscillator, respectively, and sgn$(\bullet)$ is the sign function. Actually, the form of transformations in Ref. [25] which can be used to analyze impact systems with arbitrary restitution coefficients of $0<x<1$.

According to Eq. (2), equation (1b) is converted to

$$\dot{y}_+=r\dot{y}_-, \quad \text{at} \quad y(t_*)=0, \tag{3}$$

where $\dot{y}_+$ and $\dot{y}_-$ represent the impact velocities before and after an impact for the converter oscillator, respectively.

Thus, the jump of converted velocity $\dot{y}$ becomes proportional $1-r$ instead of $1+r$ for the jump of original velocity $\dot{x}$. It is reasonable to use the Dirac function to introduce this jump into the equation of motion as an additional impulsive damping term.

Since $y(t_*\pm 0)=y(t_*)=0$ and $\dot{y}_\pm=\dot{y}(t_*\pm 0)$, by introducing the Dirac function $\delta(y(t_*))=\delta(t-t_*)/|\dot{y}|$ and further combining with $\dot{y}(t)\delta(t-t_*)=\dot{y}(t_*)\delta(t-t_*)$, the impulsive term can be obtained

$$(\dot{y}_--\dot{y}_+)\delta(t-t_*)=(1-r)\dot{y}|\dot{y}|\delta(y). \tag{4}$$

According to Eqs. (3) and (4), equation (1) can be changed into

$$\begin{aligned}&\ddot{y}+\omega_0^2y+(c_2(|y|-h)^2-c_1)\dot{y}\\&-\omega_0^2h\mathrm{sgn}y+c_3(|y|-h)^3\mathrm{sgn}y\\&=f\cos(\Omega t)\mathrm{sgn}y-(1-r)\dot{y}\,|\dot{y}|\,\delta(y).\end{aligned} \tag{5}$$

Therefore, the original system with impact is reduced to one without impact expressed by Eq. (5).

3. Analysis by Krylov–Bogoliubov averaging method

For the necessity of the Krylov-Bogoliubov averaging method, we may assume that the parameter c_1, c_2, c_3, h, and $1-r$ are all small and proportional to a small parameter, then the asymptotic method of averaging to one period can be used to analyze Eq. (5). Considering the subharmonic response, then the frequency Ω of external excitation is near the resonance frequency $2\omega_0$ ($\Omega\approx 2h\omega_0$),

$$\Omega=2n\omega_0+\eta, \tag{6}$$

where η is a detuning parameter. Moreover, it also assumes that η is small and proportional to a small parameter.

In order to use the averaging method, the following transformation is used to Eq. (5):

$$y=a(t)\sin\Phi(t), \quad \dot{y}=\omega_0a(t)\cos\Phi(t), \tag{7}$$

where $\Phi(t)=(\Omega t-\varphi(t))/2n$ and $\varphi(t)$ is a new slowly varying phase shift. Therefore, equation (5) can be transformed to first-order equations as follows:

$$\begin{aligned}a'=&-c_2(|a\sin\Phi|-h)^2a\cos^2\Phi+c_1a\cos^2\Phi\\&+\omega_0h\mathrm{sgn}(\sin\Phi)\cos\Phi\\&-(1-r)a\cos^2\Phi\,|\omega_0a\cos\Phi|\,\delta(a\sin\Phi)\\&-\frac{c_3}{\omega_0}(|a\sin\Phi|-h)^3\mathrm{sgn}(\sin\Phi)\cos\Phi\\&+\frac{f}{\omega_0}\cos(2n\Phi+\varphi)\mathrm{sgn}(\sin\Phi)\cos\Phi,\end{aligned} \tag{8}$$

$$\begin{aligned}\varphi'=&\eta-2nc_2(|a\sin\Phi|-h)^2\sin\Phi\cos\Phi+2nc_1\sin\Phi\cos\Phi\\&+\frac{2n}{a}\omega_0h\mathrm{sgn}(\sin\Phi)\sin\Phi\\&-2n(1-r)\sin\Phi\cos\Phi\,|\omega_0a\cos\Phi|\,\delta(a\sin\Phi)\\&-\frac{2n}{\omega_0a}c_3(|a\sin(\Phi)|-h)^3\mathrm{sgn}(\sin\Phi)\sin\Phi\\&+\frac{2n}{\omega_0a}f\cos(2n\Phi+\varphi)\mathrm{sgn}(\sin\Phi)\sin\Phi,\end{aligned} \tag{9}$$

where $a'=\mathrm{d}a/\mathrm{d}t$, $\varphi'=\mathrm{d}\varphi/\mathrm{d}t$.

The right sides of Eqs. (8) and (9) are proportional to a small parameter, the derivatives a' and φ' are both small under the assumption that c_1, c_2, c_3, h, and $1-r$ are all small, then a and φ are slowly varying random processes with respect to time t, and $\Phi$is a fast varying random progress. The average

procedure is applied to this system over the fast state variables Φ, and then the following equations can be derived:

$$\begin{aligned} a' &= \frac{c_1}{2}a - \frac{c_2h^2}{2}a + \frac{(r-1)\omega_0}{\pi}a + \frac{4c_2h}{3\pi}a^2 \\ &\quad - \frac{c_2}{8}a^3 - \frac{4nf\sin\varphi}{(4n^2-1)\omega_0\pi}, \end{aligned} \tag{10}$$

$$\begin{aligned} \varphi' &= \frac{4n\omega_0 h}{\pi a} + \frac{4nc_3h^3}{\omega_0\pi a} + \eta - \frac{3nc_3h^2}{\omega_0} + \frac{8nc_3h}{\omega_0\pi}a \\ &\quad - \frac{3nc_3}{4\omega_0}a^2 - \frac{4nf\cos\varphi}{(4n^2-1)\omega_0\pi a}. \end{aligned} \tag{11}$$

The steady-state solutions of Eqs. (10) and (11) are considered. Let$a = a_0$, $\varphi = \varphi_0$, $a' = 0$, and $\varphi' = 0$, then we can obtain the equations that the steady-state solutions of Eqs. (10) and (11) satisfy as follows:

$$\begin{aligned} &\frac{c_1}{2}a_0 - \frac{c_2h^2}{2}a_0 + \frac{(r-1)\omega_0}{\pi}a_0 + \frac{4c_2h}{3\pi}a_0^2 - \frac{c_2}{8}a_0^3 \\ &= \frac{4nf\sin\varphi_0}{(4n^2-1)\omega_0\pi}, \end{aligned} \tag{12}$$

$$\begin{aligned} &\frac{4n\omega_0 h}{\pi} + \frac{4nc_3h^3}{\omega_0\pi} + \eta a_0 - \frac{3nc_3h^2}{\omega_0}a_0 + \frac{8nc_3h}{\omega_0\pi}a_0^2 - \frac{3nc_3}{4\omega_0}a_0^3 \\ &= \frac{4nf\cos\varphi_0}{(4n^2-1)\omega_0\pi}. \end{aligned} \tag{13}$$

According to Eqs. (12) and (13), the frequency response equation can be derived as

$$\begin{aligned} &\left(\frac{c_1}{2}a_0 - \frac{c_2h^2}{2}a_0 + \frac{(r-1)\omega_0}{\pi}a_0 + \frac{4c_2h}{3\pi}a_0^2 - \frac{c_2}{8}a_0^3\right)^2 \\ &+ \left(\frac{4n\omega_0 h}{\pi} + \frac{4nc_3h^3}{\omega_0\pi} + \eta a_0 - \frac{3nc_3h^2}{\omega_0}a_0 \right. \\ &\left. + \frac{8nc_3h}{\omega_0\pi}a_0^2 - \frac{3nc_3}{4\omega_0}a_0^3\right)^2 \\ &= \frac{16n^2f^2}{(4n^2-1)^2\omega_0^2\pi^2}. \end{aligned} \tag{14}$$

Hence, the equation of the backbone curve can be given as follows:

$$\begin{aligned} &\frac{4n\omega_0 h}{\pi} + \frac{4nc_3h^3}{\omega_0\pi} + \eta a_0 - \frac{3nc_3h^2}{\omega_0}a_0 \\ &+ \frac{8nc_3h}{\omega_0\pi}a_0^2 - \frac{3nc_3}{4\omega_0}a_0^3 = 0. \end{aligned} \tag{15}$$

By finding the intersection of the backbone curve and the frequency response curve, the peak amplitude can be derived.

For given parameters of system (1), equation (14) can be solved by a numerical method. We introduce the perturbation terms which can be used to examine the stability of the steady-state solutions,

$$a = a_0 + \Delta a(t), \quad \varphi = \varphi_0 + \Delta\varphi(t), \tag{16}$$

where a_0 and φ_0 are governed by Eqs. (12)–(14), Δa and $\Delta\varphi$ are perturbation terms.

Substituting Eq. (16) into Eqs. (10) and (11) and neglecting the nonlinear terms, we obtain the linearization modulation of Eqs. (10) and (11) as follows:

$$\begin{aligned} \Delta a' &= \left(\frac{c_1}{2} - \frac{c_2h^2}{2} + \frac{(r-1)\omega_0}{\pi} + \frac{8c_2ha_0}{3\pi} - \frac{3c_2a_0^2}{8}\right)\Delta a \\ &\quad - \frac{4nf\cos\varphi_0}{(4n^2-1)\omega_0\pi}\Delta\varphi, \end{aligned} \tag{17}$$

$$\begin{aligned} \Delta\varphi' &= \left(-\frac{4n\omega_0 h}{\pi a_0^2} - \frac{4nc_3h^3}{\omega_0\pi a_0^2} + \frac{8nc_3h}{\omega_0\pi} \right. \\ &\quad \left. - \frac{3nc_3a_0}{2\omega_0} + \frac{4nf\cos\varphi_0}{(4n^2-1)\omega_0\pi a_0^2}\right)\Delta a \\ &\quad + \frac{4nf\sin\varphi_0}{(4n^2-1)\omega_0\pi a_0}\Delta\varphi. \end{aligned} \tag{18}$$

According to the characteristic equation of the coefficient matrix of Eqs. (17) and (18), the necessary and sufficient condition of the stability of the steady-state solutions a_0 and φ_0 is that the real parts of the eigenvalues of the coefficient matrix are less than zero. Due to Routh–Hurwitz rule,[26] it needs to satisfy

$$\begin{cases} \Sigma_1 = I_1 + I_4 < 0, \\ \Sigma_2 = I_1I_4 - I_2I_3 > 0, \end{cases} \tag{19}$$

where

$$\begin{aligned} I_1 &= c_1/2 - c_2h^2/2 + (r-1)\omega_0/\pi + 8c_2ha_0/3\pi - 3c_2a_0^2/8, \\ I_2 &= -4n\omega_0 h/\pi - 4nc_3h^3/(\omega_0\pi) - \eta a_0 + 3nc_3h^2/\omega_0 \\ &\quad - 8nc_3h^3a_0^2/(\omega_0\pi) + 3nc_3a_0^3/(4\omega_0), \\ I_3 &= \eta/a_0 - 3nc_3h^2/(\omega_0a_0) + 16nc_3h/(\omega_0\pi) \\ &\quad - 9nc_3a_0/(4\omega_0), \\ I_4 &= c_1/2 - c_2h^2/2 + (r-1)\omega_0/\pi + 4c_2ha_0/3\pi - c_2a_0^2/8. \end{aligned}$$

Particularly, the stability and classification of the steady-state solutions determined by the sign of Σ_1, Σ_2, and $\Sigma_1^2 - 4\Sigma_2$ can be found in Ref. [27].

4. Numerical calculation

In this section, by combining the numerical simulation, the analytical results can be verified, the frequency response is constructed by using the fourth-order Runge–Kutta algorithm. For the non-smooth characteristic of the impact system, two types of step size to improve the computation precision are chosen. Firstly, the large time step size $t_0$can be chosen. Once the displacement x is less than or equal to $-h$, we pull back the oscillator to the former step position and integrate Eq. (1) by a small step size of $0.01t_0$. When the displacement $x \le -h$ is satisfied under the small step size of $0.01t_0$, the velocity transformation (1b) can be used to derive the new velocity and the integration step size is then recovered to t_0. In addition, from Eqs. (2) and (7), we know that

$a^2 = y^2 + (\dot{y}/\omega_0)^2 = (x+h)^2 + (\dot{x}/\omega_0)^2$. All results are obtained for the first-order subharmonic response ($n = 1$), with mean excitation frequency being close to $2\omega_0$.

The parameters of the system are listed as follows: $\omega_0 = 1.0$, $r = 0.8$, $h = 0.08$, $c_2 = 0.15$, and $f = 0.3$. Three cases of the nonlinearity intensity ($c_3 = -0.1$, $c_3 = 0.0$, and $c_3 = 0.1$) are considered, respectively. In order to confirm the existence of impact in system (1), the phase portraits of system (1) are depicted corresponding to two different cases of damping coefficient c_1, it can be seen that under these cases the response of the system should be the impact ones. In this paper, only the impact case is considered.

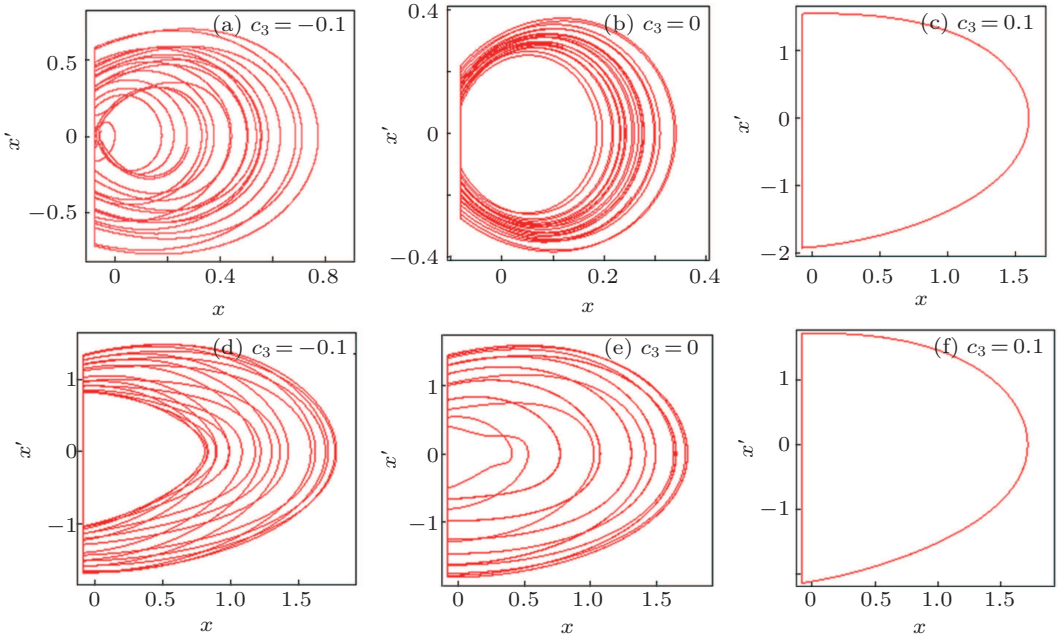


Fig. 2. (color online) Phase portraits of system (1) for $\Omega = 2.08$: (a)$c_1 = 0.1$, $c_3 = -0.1$; (b) $c_1 = 0.1$, $c_3 = 0.0$; (c) $c_1 = 0.1$, $c_3 = 0.1$; (d) $c_1 = 0.2$, $c_3 = -0.1$; (e) $c_1 = 0.2$, $c_3 = 0.0$; (f) $c_1 = 0.2$, $c_3 = 0.1$.

4.1. Response characteristic for different damping parameters

In the first case, damping coefficient $c_1 = 0.1$ is considered. In Fig. 3, steady-state response curves defined by Eq. (14) are plotted for different values of excitation amplitude corresponding to three different cases of c_3. Obviously, when f is smaller (in Fig. 3 for $f = 0.1$), the system response is double-valued: one is stable while the other is unstable. This kind of response only occurs in the lower frequency region, since in the higher frequency region equation (14) only has complex solutions, which means that the system does not have steady-state solutions. In Table 1, the maximum frequencies for double-valued responses are presented corresponding to three different values of nonlinear intensity c_3 as $f = 0.1$. However, it is worth noting that when excitation amplitude f is larger (in Fig. 3 for $f = 0.3$), the system response is the traditional frequency response and with jump phenomenon in the case of $c_3 = -0.1$ and $c_3 = 0.1$. There exists a critical value $f = 0.24$ between the traditional frequency response and the double-valued response. As shown in Fig. 3, when $f = 0.24$ there is a branch of the response curve is close to zero. For the softening type (in Fig. 3(b) for $c_3 = -0.1$), this branch only appears in the higher frequency branch ($\Omega > 2$); for the hardening type (in Fig. 3(c) for $c_3 = 0.1$), it exists in the lower frequency branch ($\Omega < 2$); however, for the linear type (in Fig. 3(a) for $c_3 = 0.0$), it distributes in the whole frequency axis. Additionally, the steady-state numerical results confirm a very good accuracy of the analytical ones.

Table 1. Critical values of excitation frequency Ω for the boundary of two steady-state solutions.

c_3	–0.1	0.0	0.1
Ω	1.888	1.932	2.008

The effectiveness discussed above is also verified by the stability boundaries, the dash lines as shown in Fig. 3, which are derived by the inequality (19). In the case of $c_1 = 0.1$, Σ_1 is negative in the whole Ω– a_0 plane. Hence, only the steady-state solutions in the interior regions of the dash lines, namely, the shaded regions $\Sigma_2 < 0$ are unattainable. Moreover, the backbone curve given by Eq. (15) is also plotted in Fig. 3 by the dash-dotted lines, where the change of its shape and position can be seen.

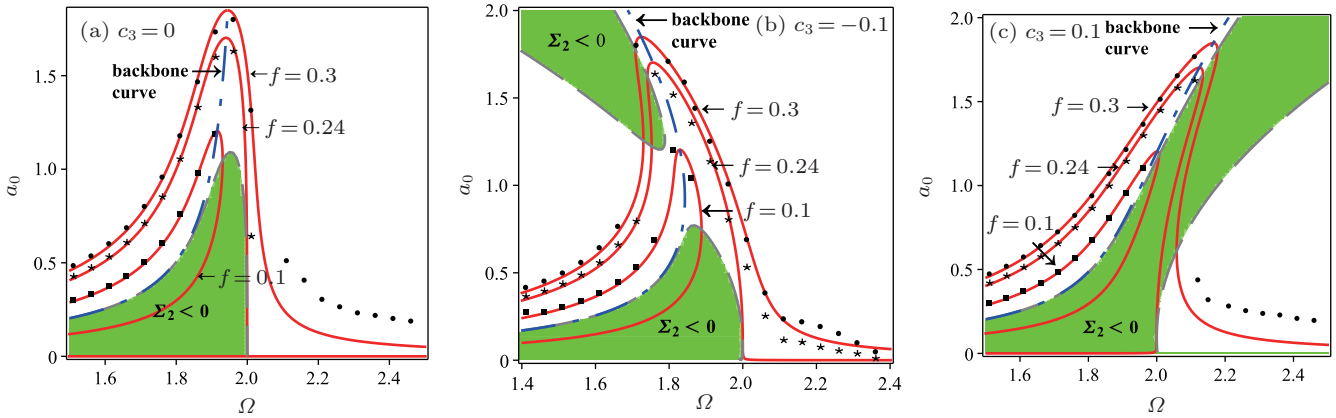


Fig. 3. (color online) Steady-state responses of system (1): (a) $c_1 = 0.1$, $c_3 = 0.0$; (b) $c_1 = 0.1$, $c_3 = -0.1$; (c) $c_1 = 0.1$, $c_3 = 0.1$. Solid lines: analytical results; the marks of ■, ∗, and •: numerical results; dashed line: stability boundaries; and dash-dotted lines: Backbone curves.

As a comparison, figure 4 depicts the response characteristic of the vibro-impact system when damping coefficient $c_1 = 0.2$. It can be seen that when the excitation amplitude is smaller (such as $f = 0.05$), the frequency response curve is separated into two parts, which is the frequency island phenomenon. Actually, this also leads to the occurrence of the four-valued response as shown in Fig. 4(d) (the local amplification of Fig. 4(b)) in the interval of $\Omega \in [1.745, 1.833]$ for $f = 0.05$; when $\Omega$is smaller than 1.745, the response keeps two-valued. As indicated in Table 2, the response characteristic for $f = 0.05$ is denoted as 2S–4S–2S–0S (nS denotes that the numbers of steady-state solutions are n). It can be seen that in the case of $f = 0.2$, there also exists a smaller interval $\Omega \in [1.642, 1.763]$ (Fig. 4(d)), in which the response is four-valued. However, for the linear like type ($c_3 = 0.0$) and the hardening type ($c_3 = 0.1$), there only exists the two-valued response for $f = 0.05$ as well as $f = 0.2$, as shown in Figs. 4(a) and 4(c).

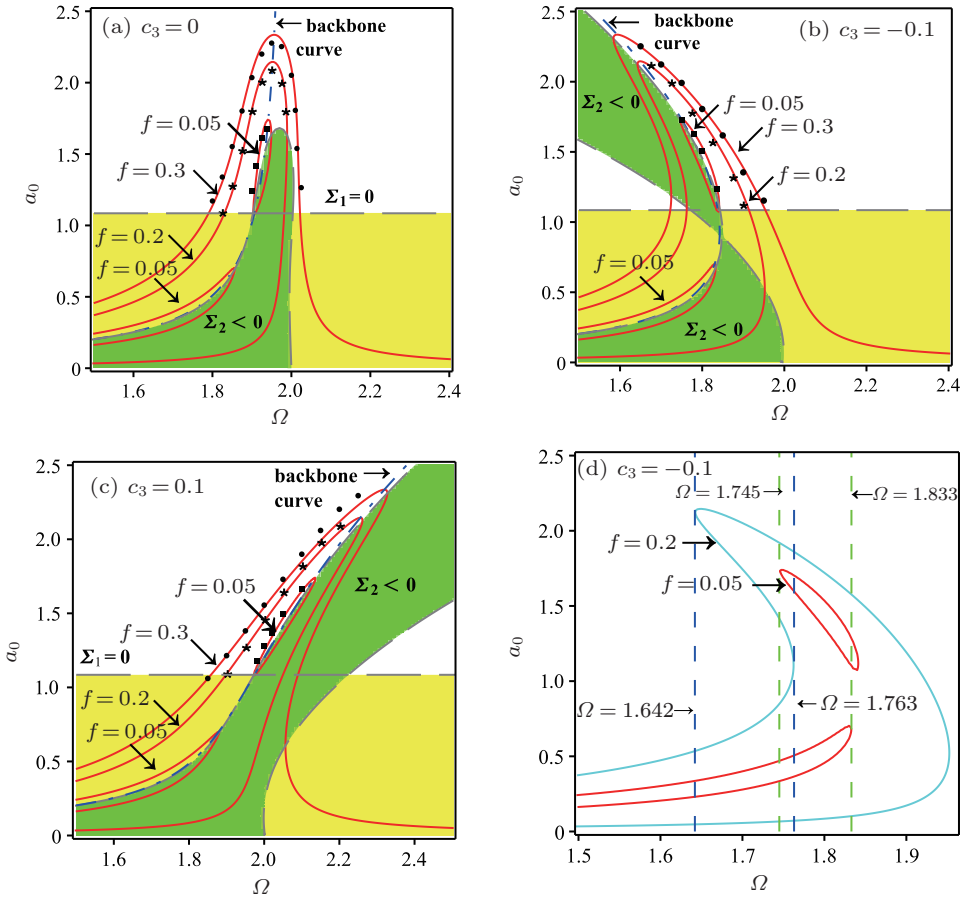


Fig. 4. (color online) Steady-state responses of system (1): (a) $c_1 = 0.2$, $c_3 = 0.0$; (b) $c_1 = 0.2$, $c_3 = -0.1$; (c) $c_1 = 0.2$, $c_3 = 0.1$. Solid lines: analytical results; the marks of ■, ∗, and •: numerical results; dashed line: stability boundaries; and dash-dotted lines: Backbone curves.

Table 2. Multi-valued response characteristic of the system for $c_1 = 0.2$.

c_3	f	Interval of excitation frequency Ω for corresponding numbers of the steady-state solutions				Response characteristic
		one or two	zero or two or three or four	one or two	zero	
–0.1	0.05	[0.0,1.745]	[1.745,1.833]	[1.833,1.842]	[1.842, +∞)	2S–4S–2S–0S
	0.2	[0.0,1.642]	[1.642,1.763]	[1.763,1.954]	[1.954, +∞)	2S–4S–2S–0S
	0.3	[0.0,1.584]	[1.584,1.725]	[1.725, +∞)		1S–3S–1S
0.0	0.05	[0.0,1.856]	[1.856,1.904]	[1.904,1.949]	[1.949, +∞)	2S–0S–2S–0S
	0.2	[0.0,1.990]	[1.990, +∞)			2S–0S
	0.3	[0.0, +∞)				1S
0.1	0.05	[0.0,1.882]	[1.882,1.975]	[1.975,2.137]	[2.137, +∞)	2S-0S–2S–0S
	0.2	[0.0,2.264]	[2.264, +∞)			2S–0S
	0.3	[0.0,2.057]	[2.057,2.329]	[2.329, +∞)		1S–3S–1S

As a result, the stability characteristic is also very different from the case of $c_1 = 0.1$. Only the steady-state solutions above the dash line $\Sigma_1 = 0$ and outside the region $\Sigma_2 < 0$ are attainable, which is similar to the results derived in Ref. [28]. As can be seen that for the frequency island response only the branch with the largest amplitude is stable and the steady-state solutions on the mainland are unstable, which is different from the case shown in Ref. [29]. These findings are checked numerically by carrying out direct integration of system (1) and a good agreement can be found between the numerical results and the analytical ones.

4.2. Analysis of the classification of the steady-state solutions in Section 4.1

As discussed in Section 3, the responses are quite different for different damping coefficient c_1 and nonlinear stiffness c_3; therefore, the classification of the steady-state solutions is also very different. In the following part, it can be analyzed specifically.

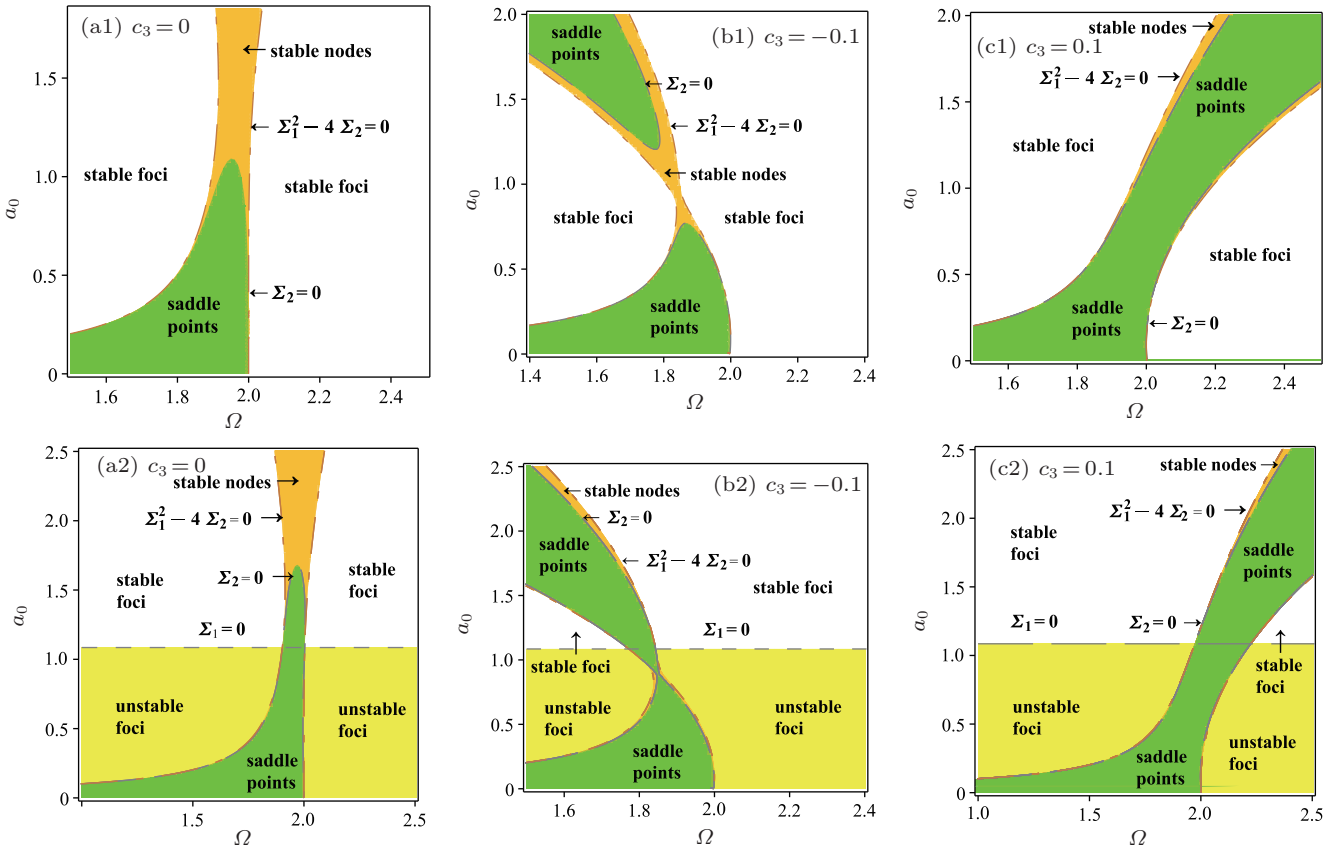


Fig. 5. (color online) Classification of the steady-state solutions: (a1) $c_1 = 0.1$, $c_3 = 0.0$; (b1) $c_1 = 0.1$, $c_3 = -0.1$; (c1) $c_1 = 0.1$, $c_3 = 0.1$; (a2) $c_1 = 0.2$, $c_3 = 0.0$; (b2) $c_1 = 0.2$, $c_3 = -0.1$; (c2) $c_1 = 0.2$, $c_3 = 0.1$.

The stability classification[27] is illustrated in Fig. 5, where the critical stability boundaries divide the plane into stable and unstable regions. Comparing Figs. 5(a1), 5(b1), and 5(c1) with Figs. 5(a2), 5(b2), and 5(c2) indicates that the damping coefficient can cause a drastic change in the response characteristic. Through the boundary $\Sigma_2 = 0$, the steady-state solutions lose stability via a saddle node bifurcation, and they are saddle points interior the boundary $\Sigma_2 = 0$. Above the dash line $\Sigma_1 = 0$ as well as outside the saddle points region, the steady-state solutions are stable, which include stable nodes and stable foci; and the critical boundary $\Sigma_1^2 - 4\Sigma_2 = 0$ is the division line for nodes and foci. However, the critical boundary Σ_1 corresponding to the occurrence of Hopf bifurcation keeps unchanged in spite of different values of nonlinearity intensity c_3. The non-trivial solutions lose stability via a Hopf bifurcation yielding aperiodic response.

4.3. Response analysis according to the jump avoidance condition

In previous sections, the existence of the saddle node bifurcation which results in the jump phenomenon is found. A jump will occur as long as there are two points on the steady-state response curve with a vertical slope,[30–32] corresponding to $\mathrm{d}\Omega/\mathrm{d}a_0 = 0$. The jump can be avoided if it can be ensured that the frequency response of the system is unique. According to Eq. (14), we have

$$\eta^2 + 2I_5\eta + I_5^2 - I_6 = 0, \tag{20}$$

where

$$\begin{aligned} I_5 &= 4n\omega_0 h/(\pi a_0) + 4nc_3h^3/(\omega_0\pi a_0) - 3nc_3h^2/\omega_0 \\ &\quad + 8nc_3ha_0/(\omega_0\pi) - 3nc_3a_0^2/(4\omega_0), \\ I_6 &= 16n^2f^2/\left[(4n^2-1)^2\omega_0^2\pi^2a_0^2\right] - I_4^2. \end{aligned}$$

Then, the excitation frequency can be derived as follows:

$$\Omega = 2\omega_0 - I_5 \pm \sqrt{I_6}. \tag{21}$$

Differentiating both sides of Eq. (21) with respect to $a_0$and substituting $\mathrm{d}\Omega/\mathrm{d}a_0 = 0$ yield

$$I_7 \pm \frac{1}{2\sqrt{I_6}}\left(\frac{-32n^2f^2}{(4n^2-1)^2\omega_0^2\pi^2a_0^3} - 2I_4I_8\right) = 0, \tag{22}$$

where

$$\begin{aligned} I_7 &= 4n\omega_0 h/(\pi a_0^2) + 4nc_3h^3/(\omega_0\pi a_0^2) \\ &\quad - 8nc_3h/(\omega_0\pi) + 3nc_3a_0/(2\omega_0), \\ I_8 &= 4c_2h/(3\pi) - c_2a_0/4. \end{aligned}$$

According to Eq. (22), figure 6 depicts the critical amplitude a_0 as a function of excitation amplitude f for $c_1 = 0.1$ and $c_1 = 0.2$, respectively. These results also verify the characteristic shown in Figs. 2 and 3. It can be seen that for $c_3 = 0.0$ and $c_1 = 0.1$ (Fig. 6(a1)), as f is smaller than 0.24, there is one point satisfying $\mathrm{d}\Omega/\mathrm{d}a_0 = 0$, which is due to the two-valued response characteristic. Then, as f is greater than 0.24, there is no critical amplitude (Fig. 6(a1)), and therefore no jump. Hence, $f = 0.24$ is the maximum and acceptable value of f in practical design to avoid the jump for $c_3 = 0.0$ and $c_1 = 0.1$.

Next, as shown in Fig. 6(a2) for $c_3 = 0.0$ and $c_1 = 0.2$, in the interval of $f \in [0, 0.054]$, there are three points satisfying $\mathrm{d}\Omega/\mathrm{d}a_0 = 0$, which is induced by the two-valued response with frequency island phenomenon. Then, in the interval of $f \in [0.054, 0.24]$, there is one point satisfying $\mathrm{d}\Omega/\mathrm{d}a_0 = 0$ corresponding to the complete two-valued response without frequency island. However, in the interval of $f \in [0.24, 0.26]$, there still exist two points satisfying $\mathrm{d}\Omega/\mathrm{d}a_0 = 0$. This is due to the existence of traditional frequency response with jump phenomenon, such as the example shown in Fig. 7(a) for$f = 0.25$. When$f$is greater than 0.26, there is no critical amplitude for $c_3 = 0.0$ and $c_1 = 0.2$ (Fig. 6(a2)), and therefore no jump.

For $c_3 = -0.1$ and $c_1 = 0.1$, as shown in Fig. 6(b1), there exist two branches, the points in the lower amplitude correspond to the two-valued response, while the branch in the higher amplitude is relative to the traditional frequency response with jump phenomenon. Particularly, in the interval $f \in [0.152, 0.24]$, there exist three points satisfying $\mathrm{d}\Omega/\mathrm{d}a_0 = 0$ for every value of f. Actually, corresponding to certain value of f, the response is four-valued, such as the example shown in Fig. 7(b) for $f = 0.2$. For $c_3 = -0.1$ and $c_1 = 0.2$, as shown in Fig. 6(b2), when f is smaller than 0.24 there always exists the four-valued response. Therefore, it has three points satisfying $\mathrm{d}\Omega/\mathrm{d}a_0 = 0$. When f is greater than 0.24, there exist two points satisfying $\mathrm{d}\Omega/\mathrm{d}a_0 = 0$, which corresponds to the response with jump phenomenon.

For $c_3 = 0.1$ and $c_1 = 0.1$, as shown in Fig. 6(c1), in the interval $f \in [0.0, 0.24]$, it is pure two-valued response. For $c_3 = 0.1$ and $c_1 = 0.2$, as shown in Fig. 6(c2), in the interval $f \in [0.0, 0.055]$, the response is two-valued with frequency island phenomenon (Fig. 4(c)). Thus, there exist three points which satisfy $\mathrm{d}\Omega/\mathrm{d}a_0 = 0$. In the interval $f \in [0.055, 0.24]$, it is pure two-valued response. Both in Fig. 6(c1) and Fig. 6(c2), f is greater than 0.24, which is a traditional frequency response.

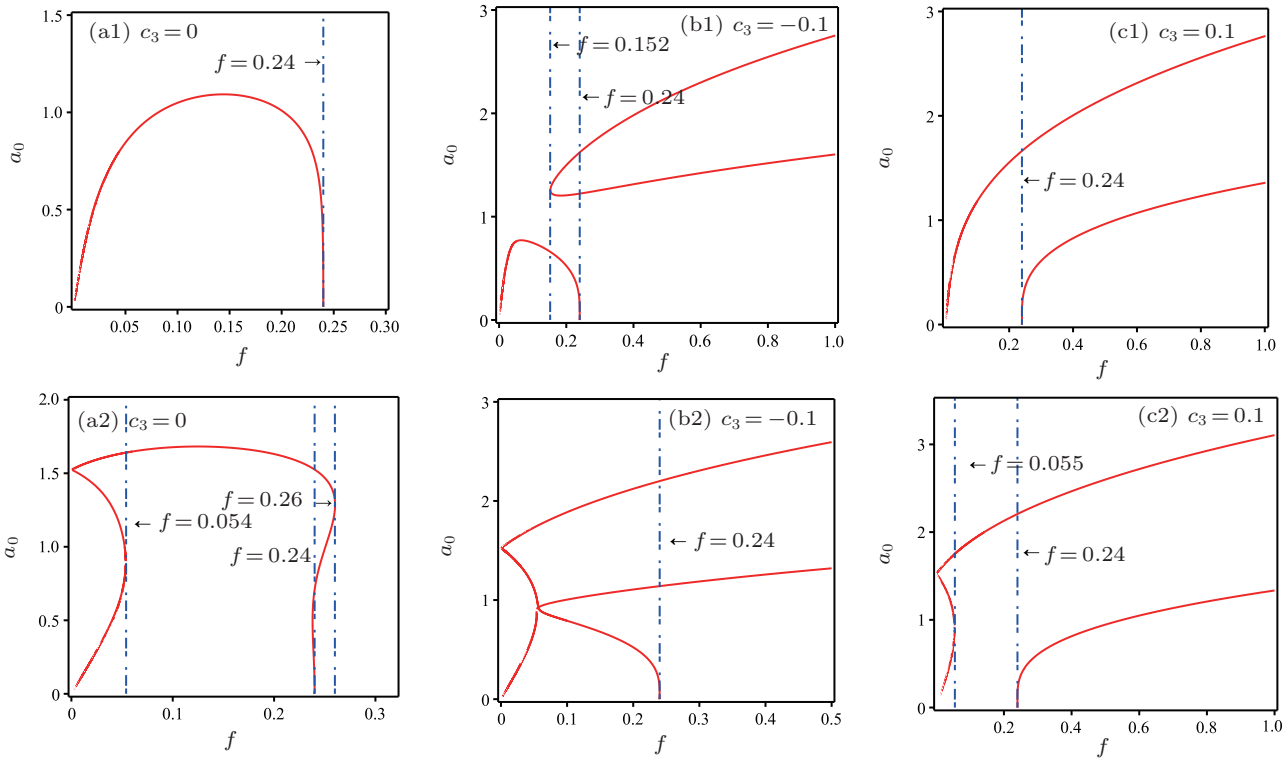


Fig. 6. (color online) Response analysis according to jump avoidance condition: (a1) $c_1 = 0.1$, $c_3 = 0.0$; (b1) $c_1 = 0.1$, $c_3 = -0.1$; (c)$c_1 = 0.1$, $c_3 = 0.1$; (a2) $c_1 = 0.2$, $c_3 = 0.0$; (b2) $c_1 = 0.2$, $c_3 = -0.1$; (c2) $c_1 = 0.2$, $c_3 = 0.1$.

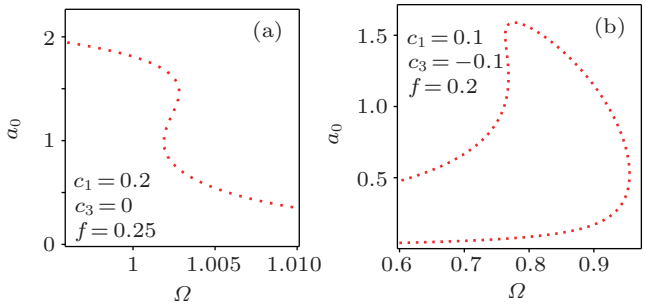


Fig. 7. (color online) Frequency response of system (1) for verifying the case in Fig. 6.

4.4. Effects of the distance between the system's static equilibrium position and the barrier on the frequency response

When the excitation frequency is fixed at $\Omega = 2.08$, the distance h is varied. The steady-state response of a_0 is shown in Fig. 8.

As can be seen that, when the nonlinear stiffness is of softening type, with the increase of the distance h, the steady-state response from the maximum value keeps decreasing to zero in spite of different values of excitation amplitude. However, when the nonlinear stiffness is of hardening type, with larger excitation amplitude, three-valued and two-valued responses can be induced. Obviously, when $f = 0.1$, with the increase of h there exists a small interval in which the response is three-valued. For $f = 0.2$ and $f = 0.3$, as described in Table 3, three-valued response and two-valued response coexist. Hence, the distance is also a very important factor to influence the response of the vibro-impact system.

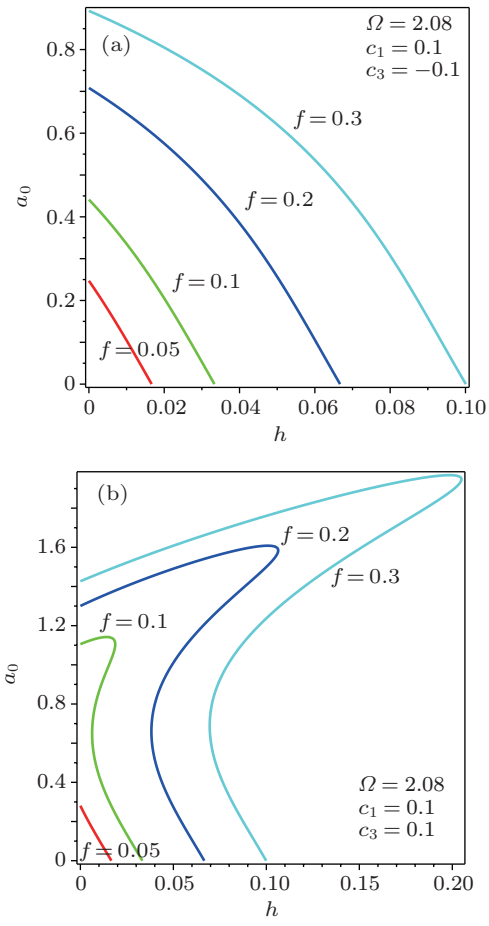


Fig. 8. (color online) Effects of the distance h on the steady-state response: (a) $c_3 = -0.1$; (b) $c_3 = 0.1$.

Table 3. Multi-valued response characteristic of the system with hardening type of stiffness.

f	The effective response interval of the distance h			The response
	One	Three	Two or one	characteristic
0.05	[0.0,0.0168]			1S
0.1	[0.0,0.0063]	[0.0063,0.0188]	[0.0188,0.0335]	1S–3S–1S
0.2	[0.0,0.0382]	[0.0382,0.0667]	[0.0667,0.1061]	1S–3S–2S
0.3	[0.0,0.0696]	[0.0696,0.1000]	[0.1000,0.2048]	1S–3S–2S

5. Conclusions

The multi-valued responses and dynamic stability of a nonlinear vibro-impact system with a unilateral non-zero offset barrier are analyzed in this paper. Using the Zhuravlev non-smooth transformation and Krylov–Bogoliubov averaging method, the frequency response, the critical equation for the stability boundary are derived. Meanwhile, the backbone curves are also obtained. Then, by combining numerical simulation, we further investigate the effects of the parameters on the responses of the vibro-impact systems. It is found that multi-valued response, especially two-valued and four-valued responses, exist in the vibro-impact system. Meanwhile, the damping coefficient can induce the frequency island phenomenon, which is verified by the direct simulation results. In addition, the condition for suppressing the jump phenomenon is derived, and by using this condition the characteristic of multi-valued response is also confirmed. The classification of the steady-state solutions is discussed. Finally, the distance between the system's static equilibrium position and the barrier can induce two-valued and three-valued responses when the nonlinear stiffness is of hardening type.

References

[1] Ibrahim R A 2014 *J. Sound Vib.* **333** 5900
[2] Ibrahim R A 2009 *Vibro-Impact Dynamics: Modeling, Mapping and Applications* (Berlin: Springer-Verlag)
[3] Thompson J M T 1983 *Proc. T. Soc. Lond. A* **387** 407
[4] Kahraman A and Singh R 1990 *J. Sound Vib.* **142** 49
[5] Ervin E K 2009 *J. Eng. Mech.* **135** 529
[6] Jing H S and Young M 1990 *Earthq. Eng. Struct. Dyn.* **19** 789
[7] Dimentberg M F and Iourtchenko D V 2004 *Nonlinear Dyn.* **36** 229
[8] Shaw S W and Holmes P J 1983 *J. Sound Vib.* **90** 129
[9] Nordmark A B 1991 *J. Sound Vib.* **145** 279
[10] Chatterjee S and Mallik A K 1996 *J. Sound Vib.* **191** 539
[11] Xie J H 1996 *Appl. Math. Mech.* **17** 65
[12] Huang Z L, Liu Z H and Zhu W Q 2004 *J. Sound Vib.* **275** 223
[13] Yin S, Zhu X P and Kaynak O 2015 *IEEE T. Ind. Electron.* **62** 1651
[14] Luo G W, Chu Y D, Zhang Y L and Zhang J G 2006 *J. Sound Vib.* **298** 154
[15] Yin S, Wang G and Yang X 2014 *Int. J. Syst. Sci.* **45** 1375
[16] Rong H W and Wang X D 2009 *Phys. Rev. E* **80** 026604
[17] Rong H W, Wang X D, Xu W and Fang T 2008 *Acta Phys. Sin.* **327** 173 (in Chinese)
[18] Rong H W, Wang X D, Xu W and Fang T 2010 *Int. J. Non-Linear Mech.* **45** 474
[19] Yin S and Huang Z H 2015 *IEEEASME T. Mech.* **20** 2613
[20] Yin S, Li X W, Gao H J and Kaynak O 2015 *IEEE T. Ind. Electron.* **62** 657
[21] Feng J Q, Xu W, Rong H W and Wang R 2009 *Int. J. Non-Linear Mech.* **44** 51
[22] Feng J Q and Xu W 2011 *Acta Phys. Sin.* **60** 080502 (in Chinese)
[23] Li C, Xu W, Wang L and Li D X 2013 *Chin. Phys. B* **22** 110205
[24] Huang D M, Xu W, Liu D and Han Q 2014 *J. Vib. Control.*
[25] Zhuravlev V F 1976 *Mech. Solids* **11** 23
[26] Schmidt G and Tondl A 1986 *Nonlinear Vibrations* (Cambridge: Cambridge University Press)
[27] Huang D M, Xu W, Xie W X and Liu Y J 2015 *Nonlinear Dyn.* **81** 641
[28] Rakaric Z and Kovacic I 2013 *Commun. Nonlinear Sci. Numer. Simul.* **18** 1888
[29] Daqaq M F and Vogl G W 2008 *Proceeding of 6th Euromech. Nonlinear Dynamics Conference* (Saint Petersburg, Russia)
[30] Deshpande S, Mehta S and Jazar G N 2006 *Int. J. Mech. Sci.* **48** 341
[31] Jazar G N, Houim R, Narimani A and Golnaraghi M F 2006 *J. Vib. Control* **12** 1205
[32] Huang D M, Xu W, Xie W X and Han Q 2015 *Chin. Phys. B* **24** 040502